Flinders UNIVERSITY

The following article appeared as: Chiari, L., Anderson, E., Tattersall, W., Machacek, J.R., Palihawadana, P., Makochekanwa, C., Sullivan, J.P., Garcia, G., Blanco, F., McEachran, R.P., Brunger, M.J. and Buckman, S.J., 2013. Total, elastic, and inelastic cross sections for positron and electron collisions with tetrahydrofuran. The Journal of Chemical Physics, 138, 074301.

and may be found at:

http://jcp.aip.org/resource/1/jcpsa6/v138/i7/p074301

http://dx.doi.org/10.1063/1.4789584

AIP | The Journal of Chemical Physics

Total, elastic, and inelastic cross sections for positron and electron collisions with tetrahydrofuran

Luca Chiari, Emma Anderson, Wade Tattersall, J. R. Machacek, Prasanga Palihawadana et al.

Citation: J. Chem. Phys. **138**, 074301 (2013); doi: 10.1063/1.4789584
View online: http://dx.doi.org/10.1063/1.4789584
View Table of Contents: http://jcp.aip.org/resource/1/JCPSA6/v138/i7
Published by the American Institute of Physics.

Total, elastic, and inelastic cross sections for positron and electron collisions with tetrahydrofuran

Luca Chiari,[1,2] Emma Anderson,[2] Wade Tattersall,[2,3] J. R. Machacek,[2] Prasanga Palihawadana,[2] Casten Makochekanwa,[2] James P. Sullivan,[2,a)] Gustavo García,[4,5] Francisco Blanco,[6] R. P. McEachran,[2] M. J. Brunger,[1,7] and Stephen J. Buckman[2,7]

[1]*ARC Centre for Antimatter-Matter Studies, School of Chemical and Physical Sciences, Flinders University, GPO Box 2100, Adelaide, SA 5001, Australia*
[2]*ARC Centre for Antimatter-Matter Studies, Research School of Physics and Engineering, The Australian National University, Canberra, ACT 0200, Australia*
[3]*ARC Centre for Antimatter-Matter Studies, School of Engineering and Physical Sciences, James Cook University, Townsville, QLD 4810, Australia*
[4]*Instituto de Física Fundamental, Consejo Superior de Investigationes Científicas (CSIC), Serrano 113-bis, 28006 Madrid, Spain*
[5]*Centre for Medical Radiation Physics, University of Wollongong, Wollongong, NSW 2522, Australia*
[6]*Departamento de Física Atómica, Molecular y Nuclear, Universidad Complutense de Madrid, 28040 Madrid, Spain*
[7]*Institute of Mathematical Sciences, University of Malaya, 50603 Kuala Lumpur, Malaysia*

(Received 14 November 2012; accepted 15 January 2013; published online 15 February 2013)

We present total, elastic, and inelastic cross sections for positron and electron scattering from tetrahydrofuran (THF) in the energy range between 1 and 5000 eV. Total cross sections (TCS), positronium formation cross sections, the summed inelastic integral cross sections (ICS) for electronic excitations and direct ionization, as well as elastic differential cross sections (DCS) at selected incident energies, have been measured for positron collisions with THF. The positron beam used to carry out these experiments had an energy resolution in the range 40–100 meV (full-width at half-maximum). We also present TCS results for positron and electron scattering from THF computed within the independent atom model using the screening corrected additivity rule approach. In addition, we calculated positron-impact elastic DCS and the sum over all inelastic ICS (except rotations and vibrations). While our integral and differential positron cross sections are the first of their kind, we compare our TCS with previous literature values for this species. We also provide a comparison between positron and electron-impact cross sections, in order to uncover any differences or similarities in the scattering dynamics with these two different projectiles. © *2013 American Institute of Physics*. [http://dx.doi.org/10.1063/1.4789584]

I. INTRODUCTION

Research on the effects of ionizing radiation in biomolecular systems has attracted intense interest, in the last decade or so, within the atomic and molecular physics and medical science communities.[1] In particular, the importance of electron-induced chemical processes at low energies has recently been highlighted by the discovery that electrons at sub-ionization[2] and even sub-excitation energies[3] can attach to and cause the fragmentation of the nucleic acids, the proteins, and their components, such as the nucleobases, the sugars, and water.[4] These processes can eventually result in important cell and tissue damage.[5,6]

Positrons can also potentially trigger damage in biomolecular systems, e.g., by the liberation of significant numbers of secondary low-energy electrons, as the positrons thermalize within the biological medium, through processes such as direct ionization.[1] However, the mechanisms leading to biological damage are qualitatively and quantitatively different for positrons and electrons.[7] In particular, the presence of the positronium (Ps) formation channel in positron impact phenomena leads to gamma rays originating from the Ps annihilation which potentially add to the ionizing effect inside the organic tissue.[7]

In fact, the detection of the annihilation radiation emitted by the positrons, as they enter the human body and annihilate with the molecular electrons, is at the heart of positron emission tomography scans, an imaging technique of metabolic activity, and an early detection tool for tumours. The application of positrons in medical science, however, has expanded to beyond purely diagnostic purposes. Indeed, they have also been employed in therapeutic or clinical procedures, e.g., as probes for protein syneresis,[8] in bioactive molecule encapsulation,[9] and even in the treatment of tumours (positherapy).[10] Nevertheless, there are many unanswered questions about the interactions of positrons with biomolecules,[11] because the science behind the processes that take place at the atomic and molecular level remains mostly unknown. As a consequence, our group has embarked on a project to explore the interaction of positrons with molecules of biological interest. This project has started with experiments on the primary constituent of all living organisms, i.e.,

a)Author to whom correspondence should be addressed. Electronic mail: james.sullivan@anu.edu.au.

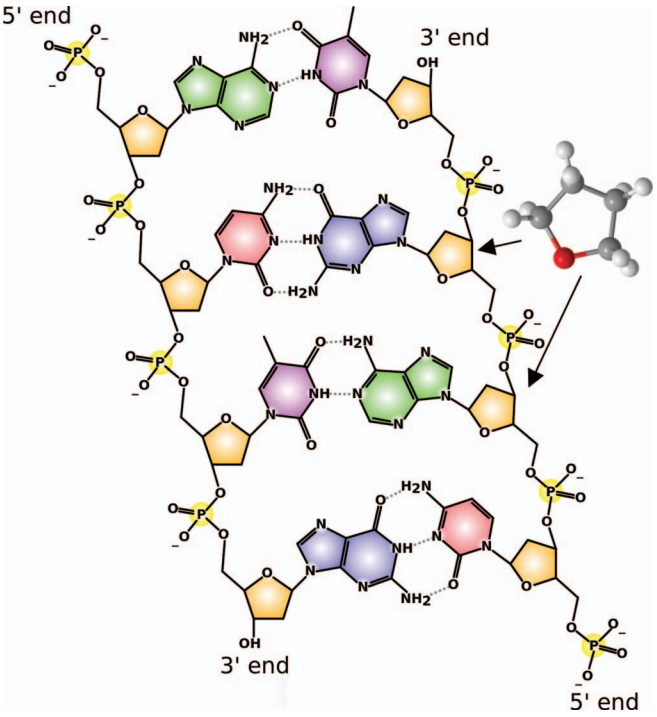

FIG. 1. Schematic diagram of an unrolled segment of DNA with the THF molecule highlighted in the phosphate-deoxyribose backbone structure.

water, and the simplest organic acid, namely, formic acid.[12] In the present study, we shift our focus to tetrahydrofuran (THF: C_4H_8O). THF represents a suitable model or analogue for the sugar rings (ribose or deoxyribose) that are contained in all nucleoside bases and which play an essential role in the structure of both DNA[13–15] and RNA.[16] In fact, as specifically shown by the schematic diagram of an unrolled segment of DNA in Figure 1, the backbone structure of the nucleic acids can be viewed as a series of THF-like molecules held together by phosphate bonds, to which the nucleobases are covalently linked to form the nucleotides. Therefore, THF can be thought of as a prototypical analogue of the building blocks for living matter.[17,18]

THF also has some physico-chemical properties that make it an interesting species to investigate from a more fundamental perspective. For example, it is a heterocyclic organic compound containing an ether group with an exposed oxygen atom available for hydrogen bonding. This peculiarity in its structure makes it one of the most polar of the simple ethers. In fact, THF possesses both a large permanent dipole moment $\mu = 1.63$ D,[19] and static dipole polarizability $\alpha = 47.08$ a.u.[18] However, THF is also known to be conformationally impure. In fact, the THF molecule comes in at least three symmetric and two asymmetric conformers[20] and this needs to be borne in mind when carrying out experiments on this target, as it may potentially complicate the interpretation of the results. Nevertheless, at room temperature the population of conformers in our THF sample is expected to be essentially dominated by nearly the same proportion of the two most energetically stable conformers, i.e., those in the C_2 (55.5%) and C_s (44.5%) geometry.[21] It is interesting to note that these two lowest energy conformers share the same values for the dipole moment and the dipole polarizability (see above).[18] Therefore, the presence of more than one conformer in our THF sample might not significantly complicate the interpretation of our experimental results.

Given its interesting properties, and the biological role of THF that we have outlined above, it is not surprising to find a considerable number of papers in the literature on low-energy electron collisions with this target. In particular, we note the total cross section (TCS) measurements of Zecca *et al.*,[22] Możejko *et al.*,[23] and Baek *et al.*[24] Elastic differential cross section (DCS) measurements at selected impact energies have been carried out by Milosavljević *et al.*,[25] Allan,[26] Colyer *et al.*,[27] Dampc *et al.*,[28] Gauf *et al.*,[29] and Baek *et al.*[24] Except for the work of Milosavljević *et al.*,[25] these groups also reported elastic integral cross sections (ICS). To the best of our knowledge, the only electron-impact, discrete electronic-state excitation cross sections are those of Do *et al.*,[30] while a review of all the available earlier work and a recommended database for electron-THF scattering can be found in Fuss *et al.*[31] Among the theoretical studies on electron-THF scattering, we note the TCS calculation using the *R*-matrix method of Bouchiha *et al.*[32] Computations of the elastic DCS have been reported by Możejko and Sanche[33] with the independent atom model (IAM), Trevisan *et al.*[34] using the complex Kohn variational method, and Winstead and McKoy[35] and Gauf *et al.*[29] both employing the Schwinger multichannel method (SMC). These authors, with the exception of Trevisan *et al.*,[34] calculated the elastic ICS as well. For completeness, we also cite the elastic ICS computation by Tonzani and Greene[36] using the *R*-matrix approach.

With positron projectiles, however, there is only one earlier experimental investigation on THF from the group at the University of Trento[22] and there are no calculated cross sections. From a theoretical point of view, this reflects the difficulty in making an accurate quantum-mechanical description of a large target molecule such as THF, as well as the difficulties posed by incorporating Ps formation into the formalism.

In this paper, we report on measurements of the TCS and Ps formation cross section for positron scattering from THF in the energy range from 1 to 190 eV. In addition, the summed inelastic ICS for electronic excitations and direct ionization have been measured up to 20 eV. Furthermore, measurements of elastic DCS at selected incident energies between 1 and 25 eV are also described. The experiments were carried out at the Australian Positron Beamline Facility,[37] using a positron beam with an energy resolution in the range 40–100 meV (full-width at half-maximum). In order to partially fill the gap in the theoretical results for positron scattering from THF, we have also computed the TCS, the elastic ICS and the sum over all inelastic ICS (except for rotations and vibrations) within the IAM approach with screening (SCAR) corrections applied. The energy range of these computations is between 1 and 5000 eV. In addition, in order to facilitate a comparison of the cross sections for positron and electron collisions with THF, we report on new theoretical results for electron scattering from this target species, calculated with the same method and in the same energy range.

In Sec. II of this paper, we discuss the experimental procedures of our measurements, and Sec. III presents the

positron and electron scattering models and the computational details that we employed in our calculations. We then report and discuss our results in Sec. IV, before drawing some conclusions from the present investigation.

II. EXPERIMENTAL DETAILS

The measurements presented here were carried out using the low-energy positron beamline at the Australian National University. This apparatus is based on a "Surko" trap and beam system[38] and has already been described in detail in Ref. 37, so that only an overview of its operation will be presented here. Positrons are obtained from a ^{22}Na radioactive isotope, which had an activity of approximately 40 mCi for the present measurements. A solid neon moderator is used to moderate the high-energy positrons emitted by this source. The low-energy positron beam is then radially confined using a solenoidal magnetic field (100 G), and is transported into a two-stage buffer-gas trap where a uniform and strong magnetic field (530 G) is present. The trap electrodes form a stepped electrostatic potential well structure, so that the positrons that lose energy through inelastic collisions with a mixture of N_2 and CF_4 buffer gases are trapped inside the well. In this process, the positrons thermalize to room temperature and form a cloud of particles that becomes the reservoir for the formation of a pulsed positron beam. The trap is typically operated at a repetition rate of 60–100 Hz with up to ∼1000 positrons emitted in each individual pulse. The positrons released by the trap are directed into a scattering cell where they interact with the molecules of the target of interest, THF in this case. The scattering cell is made of gold-plated copper and is 20 cm long, with entrance and exit apertures that are 5 mm in diameter. The strong magnetic fields (530 G) present in the scattering cell region, and downstream from it, ensure that all the positrons, except for those positrons that form Ps and annihilate within the cell, are transmitted. Those positrons subsequently pass through a retarding potential analyzer (RPA), which is sensitive only to the parallel energy component ($E_\parallel$) of the beam. The positrons transmitted by the RPA are finally detected by a double-stack, micro-channel plate assembly.

In our experimental configuration, the incident energy, at which the positrons scatter from the target molecules, is set by the potential of the scattering cell. The zero for the energy scale is established with a retarding potential analysis of the beam, i.e., with the energy scale defined relative to the "cut-off" position of the beam. With this procedure the uncertainty on the energy scale is estimated to be ±25 meV. The same retarding potential analysis enables us to estimate the energy distribution of the beam. Careful control over the beam formation in the last stage of the trap cycle allows the energy width of the beam to be comparable to the temperature of the trapped positron cloud. For these measurements, the energy resolution of the beam varied between 40 and 100 meV due to variations in the beam formation characteristics.

Several precautions need to be taken in order to accurately carry out the measurements. For instance, the target pressure inside the cell is set to a value such that the number of scattering events is no more than 10% of the unscattered beam intensity, in order to minimize multiple scattering effects. In addition, the pressure measurements inside the scattering cell need to be corrected for the thermal transpiration effect, because the scattering cell temperature (∼24 ± 2 °C) was different from the pressure gauge temperature (45 °C). The thermal transpiration correction was calculated according to the model of Takaishi and Sensui,[39] and was ∼3% in the magnitude of the measured cross sections. The value for the molecular diameter of THF that we used in this correction was 4.63 Å.[28] Throughout the present measurements we used a high-purity (>99.86%) THF sample. Although THF is a liquid at room temperature, it is volatile enough (vapour pressure ∼176 hPa at 25 °C)[40] to easily provide the gas number density in the cell to achieve the required beam attenuation. Note that THF is rather hygroscopic,[22] but it comes as a mostly anhydrous sample from the supplier. We also performed numerous freeze-pump-thaw cycles, in order to degas the target sample and remove any impurities present in that sample that might affect the results of our measurements.

The basic principle behind the TCS measurements, in all linear transmission scattering experiments, is the Beer-Lambert attenuation law. This method allows one to derive the TCS from attenuation measurements of the beam intensity, the target pressure in the cell, and the length of the interaction region. The techniques used in the present experiment to measure the TCS, the Ps formation cross sections, the elastic DCS, and the details of the data analysis, have been presented previously.[41–43] In short, the various cross sections are determined by measuring specific fractions of the positron beam transmitted through the RPA with the target vapor present in the scattering cell. In a collision with a target molecule, the positron can be elastically scattered through some angle θ and lose some of its $E_\parallel$ in the process. It can also lose some of its total energy if inelastic processes, such as electronic excitations or direct ionization, are energetically allowed. As the RPA discriminates against $E_\parallel$ only, a retarding potential analysis provides a simple measurement of the total scattering. We note here that, owing to our finite beam energy resolution, we cannot resolve rotations and many of the vibrational modes from the elastic scattering channel and, therefore, we actually make measurements of the quasi-elastic DCS. Ps formation is also possible above the Ps formation threshold (E_{Ps}). As the first adiabatic ionization potential (E_i) of the most stable conformer of THF is 9.57 eV,[44] and since $E_{Ps} = E_i - 6.8$ eV, we obtain that $E_{Ps} = 2.77$ eV for THF. Note that Ps formation is a loss process, so it manifests as a loss of positron intensity in the RPA transmission curve.

As with any experiment based on a linear transmission technique, our method suffers from some angular discrimination limitations. They arise from the inability to distinguish between positrons that are elastically scattered at small forward angles from those in the primary, unscattered beam. The fact that the number of "unscattered" events is overestimated results in a measured TCS that is underestimated with respect to its "true" value. At any given energy, the extent of this effect depends on the angular discrimination of the measurement and on the nature of the elastic DCS for the target species of interest in this forward angular region.[45] In the present measurements, the angular discrimination is not

TABLE I. Estimates of the missing angular range ($0^\circ \pm \theta_{min}$) in the present measured TCS, and of the corresponding correction for the forward angle scattering effect. That latter correction was calculated with the present IAM-SCAR elastic DCS, with Born dipole-induced rotational excitations (see Table VI), at selected positron scattering energies.

Energy (eV)	θ_{min} (deg)	Correction (%)
1	20	40
2	14	32
5	8.9	22
10	6.3	21
20	4.4	14
50	2.8	9
100	2.2	7
150	1.8	4

limited by geometrical constraints, but is rather determined by the finite extent of the energy resolution of our positron beam. In fact, our experimental techniques[41] rely on the measurements of the fraction of the transmitted positron intensity at the beam cutoff point in the retarding potential analysis. However, in practice, it is not possible to make a measurement of the beam intensity at exactly the cutoff voltage, because this also coincides with the cutoff point of the incident positron beam. Instead, we measure the positron intensity at a retarding potential voltage that is sufficiently far away from that cutoff. An offset $\Delta V \approx$ 120–150 mV (i.e., $\geq$ 3–4 standard deviations of the beam energy distribution) was used throughout the present measurements. As a consequence, the measured elastic DCS misses a range of the forward angles corresponding to that voltage offset and, in turn, the TCS excludes the contribution from the elastic DCS in that inaccessible angular range. The missing angular ranges $0^\circ \pm \theta_{min}$ and $180^\circ \pm \theta_{min}$ can be calculated using a method presented earlier,[41,43] where the angular discrimination is given by

$$\theta_{min} = \sin^{-1}\sqrt{\frac{e\Delta V}{E}}, \quad (1)$$

where e is the absolute value of the elementary charge (in atomic units) and E is the beam energy. The present estimates for the angular discrimination at selected scattering energies are listed in Table I. These energy-dependent angular discrimination values can be used, in conjunction with the elastic DCS at each respective energy, provided that these DCS are known, to correct the measured TCS for the forward angle scattering effect. This can be done, for instance, by following the approach described in Hamada and Sueoka.[46] The present measured DCS unfortunately cannot be used for this purpose, as they suffer from some missing angular ranges, as with the TCS. In principle, such elastic DCS are available from our IAM-SCAR computations (see Sec. III). However, as we shall see later in the results and discussion, the agreement between our measured and theoretical results is not uniformly good at all energies even at the TCS level. Therefore, without any independent validation of our calculated DCS, employing those elastic DCS in the manner outlined above may be premature. Hence, in general, we have not corrected our measured TCS for the forward angle scattering effect. As a consequence, the TCS that we present here (see Table II) represent a lower limit on the "real value." Nevertheless, in order to estimate the extent of this instrumental effect, we have employed our theoretical elastic DCS to calculate the correction to our measured TCS at a few selected positron energies (see Table I and Figure 2). In doing so, we find that the magnitude of the TCS we list in Table II would increase between ~40% at 1 eV and ~4% at 150 eV. Thus, as we found in our earlier investigation on the polar species water and formic acid,[12] we can expect the forward angle scattering correction to our measured TCS to be significant at the lower energies and become smaller as the positron energy increases.

In this paper, we also present measurements of elastic DCS at energies above the threshold for the first electronic-state excitation, and of the summed inelastic ICS for electronic excitations and direct ionization. The methods used in the present experiment to measure those cross sections have already been described earlier by Makochekanwa *et al.*,[42] Caradonna *et al.*,[47] and Sullivan *et al.*[43] We briefly summarize them here, by recalling that those measurements require an alteration to the experimental technique from that used in the case of quasi-elastic scattering.

The total positron energy can be expressed in terms of the components that are parallel and perpendicular to the magnetic field, $E_{tot} = E_{\parallel} + E_{\perp}$. However, at energies above the first electronic excitation, there is no longer the one-to-one relationship between $E_{\parallel}$ and θ that was valid in the case of quasi-elastic scattering. This is because any energy loss from $E_{\parallel}$ can now be due to both inelastic scattering and angular elastic scattering. We can take advantage of the fact that for a slowly varying magnetic field the magnetic moment of a charged particle ($E_{\perp}/B$) is an adiabatic invariant. Thus, by changing the ratio of the magnetic field in the scattering cell (B_{SC}) to that in the RPA (B_{RPA}), it is possible to convert some, or all, of the positron's perpendicular energy back into the parallel component. In this way, we can separate losses of $E_{\parallel}$ that are due to various discrete inelastic scattering events, from those losses that are due to the transfer of energy from $E_{\parallel}$ to $E_{\perp}$ as a result of angular elastic scattering. Note that for a given E_{tot}, the ratio B_{SC}/B_{RPA} can be appropriately selected in order to effectively achieve this splitting. The only significant side effect is a slight enlargement of the missing angular range in our measurements. For the present measurements of the elastic DCS at energies greater than 6 eV, and for the summed inelastic ICS, we used $B_{SC}/B_{RPA} = 5$.

The statistical uncertainties on the measured cross sections lie in the range 0.5%–3.8% for the TCS, while for the Ps formation cross section, the elastic DCS, and the summed inelastic ICS, they can be significantly larger (>10%) under some circumstances. There are also sources of systematic error in our measurements (e.g., the drift in the absolute pressure scale), which are estimated and accounted for, where possible, as discussed in an earlier paper.[41] The overall errors are calculated as the square root of the quadratic sum of the individual contributing errors. The total error bars on our measured TCS are found to be in the range ~1.4%–12% and are largely due to systematic uncertainties associated with our experiment. The largest source of systematic error in this study originates from the drift in the absolute pressure

TABLE II. The present measured TCS (σ_T), Ps formation cross section (σ_{Ps}) and summed inelastic ICS for electronic excitations and direct ionization (σ_I), together with their overall uncertainties ($\Delta\sigma$).

Energy (eV)	σ_T (10^{-20} m^2)	$\Delta\sigma_T$ (10^{-20} m^2)	σ_{Ps} (10^{-20} m^2)	$\Delta\sigma_{Ps}$ (10^{-20} m^2)	σ_I (10^{-20} m^2)	$\Delta\sigma_I$ (10^{-20} m^2)
1.0	72.97	1.04				
1.2	66.13	0.95				
1.4	61.46	0.89				
1.6	57.18	0.84				
1.8	54.17	0.80				
2.0	51.62	0.77				
2.2	49.74	0.75				
2.4	47.68	0.73				
2.6	46.15	0.71	0.17	0.26		
2.8	45.38	0.71	0.86	0.28		
3.0	44.62	0.69	1.66	0.27		
3.2	43.37	0.68	2.48	0.27		
3.4	42.74	0.67	2.82	0.26		
3.6	41.53	0.66	3.39	0.27		
3.8	40.88	0.65	3.30	0.27		
4.0	40.09	0.64	3.51	0.26		
4.2	39.74	0.64	3.60	0.27		
4.4	39.26	0.63	4.02	0.27		
4.6	38.67	0.62	4.15	0.27		
4.8	39.01	0.63	4.76	0.26		
5.0	38.53	0.62	5.43	0.27		
5.2	38.07	0.62	5.63	0.27		
5.4	38.16	0.61	6.25	0.27		
5.6	37.44	0.61	6.72	0.27		
5.8	37.25	0.61	6.60	0.28		
6.0	36.08	4.14	7.61	1.11		
6.5					0.73	0.40
7.0	34.44	4.05	8.90	1.19	0.70	0.44
7.5					0.40	0.41
8.0	34.73	4.07	10.10	1.31	1.22	0.43
8.5					0.39	0.41
9.0	34.18	4.01	10.41	1.34	0.97	0.42
9.5					1.68	0.47
10.0	34.81	4.08	11.63	1.46	0.51	0.41
10.5					1.61	0.47
11.0	33.03	3.88	12.09	1.51	1.60	0.47
11.5					1.95	0.48
12.0	32.92	3.87	10.81	1.38	1.50	0.45
12.5					1.95	0.48
13.0	32.44	3.81	11.44	1.44	2.37	0.51
13.5					1.94	0.48
14.0	32.08	3.77	12.08	1.51	3.01	0.57
14.5					3.58	0.62
15.0	33.15	3.89	12.24	1.52	3.26	0.66
15.5					3.86	0.64
16.0	32.12	3.77	11.69	1.47	4.23	0.75
16.5					4.64	0.71
17.0	32.31	3.80	11.15	1.41	4.49	0.79
17.5					3.92	0.65
18.0	31.70	3.73	11.79	1.49	5.30	0.88
18.5					6.13	0.86
19.0	31.10	3.66	11.13	1.42	5.34	0.90
19.5					5.50	0.81
20.0	31.10	3.66	10.62	1.36		
21.0	31.35	3.69	10.78	1.38		
22.0	31.05	3.66	10.85	1.39		
23.0	30.85	3.64	10.28	1.32		
24.0	30.76	3.63	10.01	1.31		
25.0	30.92	3.64	9.55	1.26		

TABLE II. (*Continued*.)

Energy (eV)	σ_T (10^{-20} m^2)	$\Delta\sigma_T$ (10^{-20} m^2)	σ_{Ps} (10^{-20} m^2)	$\Delta\sigma_{Ps}$ (10^{-20} m^2)	σ_I (10^{-20} m^2)	$\Delta\sigma_I$ (10^{-20} m^2)
26.0	30.39	3.59	10.08	1.31		
27.0	30.48	3.59	9.42	1.24		
28.0	30.62	3.61	9.20	1.22		
29.0	30.53	3.60	8.96	1.20		
30.0	30.29	3.57	9.41	1.23		
31.0	29.69	3.51	8.23	1.13		
32.0	30.15	3.56	8.26	1.13		
33.0	28.57	3.39	8.04	1.11		
34.0	29.23	3.45	8.77	1.18		
35.0	30.65	3.62	8.09	1.11		
36.0	29.55	3.49	7.05	1.01		
37.0	30.26	3.57	7.52	1.06		
38.0	28.90	3.42	6.44	0.94		
39.0	29.63	3.50	7.57	1.06		
40.0	29.54	3.49	7.09	1.01		
41.0	29.07	3.44	6.68	0.98		
42.0	29.19	3.46	6.20	0.95		
43.0	28.96	3.42	6.51	0.96		
44.0	29.74	3.51	5.89	0.91		
45.0	29.62	3.50	6.26	0.94		
46.0	29.48	3.48	5.95	0.92		
47.0	28.58	3.39	5.52	0.88		
48.0	29.31	3.46	5.90	0.92		
49.0	29.08	3.44	4.90	0.83		
50.0	28.98	3.43	5.24	0.87		
51.0	28.92	3.42				
52.0	28.68	3.40				
53.0	29.52	3.48				
54.0	27.26	3.24				
55.0	30.07	3.55				
56.0	28.20	3.34				
57.0	28.56	3.39				
58.0	28.76	3.40				
59.0	27.21	3.24				
60.0	28.03	3.40	4.78	0.63		
70.0	27.96	0.69	4.40	0.64		
80.0	27.40	0.70	4.01	0.64		
90.0	27.27	0.70	3.28	0.64		
100.0	26.38	0.69	2.43	0.63		
110.0	24.55	0.66	1.61	0.62		
120.0	24.12	0.65	1.16	0.60		
130.0	24.36	0.65	1.32	0.60		
140.0	24.25	0.64	1.26	0.57		
150.0	23.86	0.64	1.44	0.58		
160.0	22.63	0.64	0.73	0.58		
170.0	22.00	0.60	0.16	0.57		
180.0	21.92	0.59	0.43	0.46		
190.0	21.68	0.49	0.03	0.33		

measurements, which is independent of positron energy, and this can be significant under some circumstances.

III. THEORY DETAILS

A. Atomic optical model for electron scattering

The IAM approach within the SCAR formalism has been extensively used earlier for modeling electron scattering from a large variety of different sized molecules (from diatomics to macro-molecules),[48–51] over a broad energy range, typically from 1 to 5000 eV. Therefore, we do not repeat those details again, rather we only briefly summarize the method behind our calculations. The first subjects of our computations are the individual atoms constituting the target molecule, that is, C, H, and O in this case. Our atomic optical model approach is essentially a potential scattering approach, where the local model potential $V(r)$ is

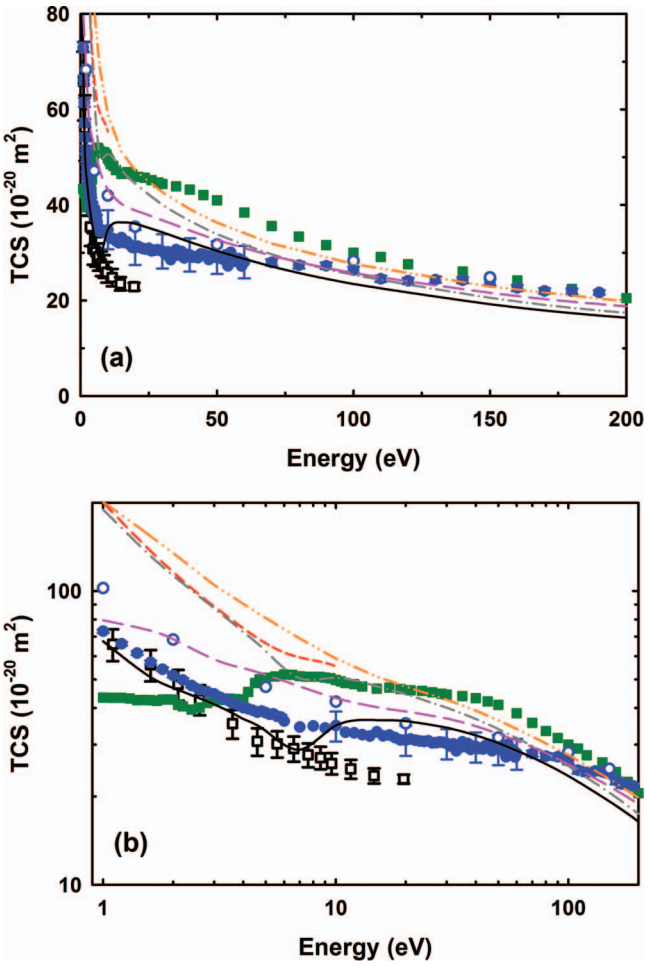

FIG. 2. (a) The present experimental TCS for positron scattering from THF (●) are compared to those from Zecca *et al.*[22] (□). Note that for clarity the overall error bars on the present experimental TCS between 6 and 60 eV are shown at some selected energies only. The present measured TCS corrected for forward angle scattering (○) are also given at selected energies (see Table I). Also plotted are the present positron (———) and electron (– – –) impact TCS calculated with our IAM-SCAR method, as well as the computed positron (– · – · – ·) and electron (– · · – · · – · ·) impact IAM-SCAR TCS also including the Born dipole-induced rotational excitations. Shown also are the electron-impact TCS measured by Mozejko *et al.*[23] (■) and computed by Bouchiha *et al.*[32] (- - -). (b) Same as (a) but in log-log scale.

taken as

$$V(r) = V_s(r) + V_{ex}(r) + V_p(r) + iV_a(r). \quad (2)$$

Here, $V_s(r)$ is the standard Hartree potential of the target. It is then supplemented by the exchange potential $V_{ex}(r)$ used by Riley and Truhlar,[52] the polarization potential $V_p(r)$ employed by Zhang *et al.*,[53] and finally the imaginary absorption potential $V_a(r)$ of Staszewska *et al.*[54] Due to the imaginary absorption potential, the optical model potential method yields a complex phase shift $\delta_l = \lambda_l + i\mu_l$. This allows for the calculation of cross sections (differential and integral) for elastic scattering, inelastic scattering (all excited and ionized states combined together), and the grand total as the sum of those integral cross sections. A recent study of elastic electron scattering from atomic-iodine[55] proved the efficacy of this approach, except at the lowest energies.

B. Atomic optical model for positron scattering

Our IAM-SCAR method for modeling positron collisions with molecules is based on the same optical potential approach we outlined above for electron impact, and has been presented in depth in our recent study on positron scattering from argon[56] and molecular oxygen.[57] In those studies, reasonable agreement was found with the reported experimental results. In addition, we have also investigated the molecular systems NO_2, N_2O, 3-hydroxy-tetrahydrofuran,[58] and pyrimidine with our IAM-SCAR approach, and while the results from those studies are waiting to be written up for publication they are generally found to be in quite reasonable agreement with the available TCS data. As a consequence, we only briefly summarize the details of our positron-impact calculations here. In this case, our approach is based on an optical model in which the local complex potential is defined as

$$V(r) = V_s(r) + V_p(r) + iV_a(r). \quad (3)$$

As in Eq. (2), the real part represents the elastic scattering process and consists of the electrostatic interaction term, $V_s(r)$, and the polarization term, $V_p(r)$, whereas the imaginary part accounts for inelastic processes which are considered as absorptions, $V_a(r)$, from the incident positron beam.

Unlike with electrons, for positron collisions the definition of the energy for the absorption threshold (Δ) becomes somewhat controversial (see Blanco and García[48,49] for details). In the case of electron scattering, Δ would be the excitation energy of the first electronic state of the atom in question. However, for positron collisions, Ps formation is a dominant inelastic scattering channel that generally becomes open at a lower energy than that of the first excited electronic level. As Ps formation cannot be explained in terms of binary collisions,[59] it cannot be explicitly introduced into the original formulation of the absorption potential as an independent inelastic process. For this reason, Reid and Wadehra[60] suggested to use the Ps formation threshold energy (Δ_p) as the absorption threshold parameter (i.e., $\Delta = \Delta_p$). This approach was later shown to somewhat overestimate the TCS at the higher energies. Hence, we define an energy dependent parameter for the absorption threshold ($\Delta(E)$) of the form

$$\Delta(E) = \Delta - (\Delta - \Delta_p)\, e^{-\left(\frac{E-\Delta_p}{E_m}\right)}. \quad (4)$$

In Eq. (4), Δ is the lowest excitation energy for the atom and E_m is a characteristic energy at which the absorption potential, without Ps formation, gives the maximum cross section (E_m = 20 eV in this case). E_m modulates the negative exponential transition between the limits $\Delta(E) = \Delta_p$ for energies around the Ps formation energy and $\Delta(E) = \Delta$ for higher energies.

The choice of the polarization potential is particularly important for positron scattering calculations, as it is the only attractive contribution to the positron-atom interaction (except for virtual Ps formation). Here, we use a new polarization potential based on that developed by McEachran *et al.*[61] for the noble gases. In particular, we employ the dipole plus quadrupole polarization potential for Ne given by McEachran *et al.*,[61] but scaled by a constant in order to give the known dipole (α_d) and quadrupole (α_q) polarizabilities of the C (α_d = 11.88 a.u., α_q = 54.76 a.u.),[62,63] H (α_d = 4.50 a.u., α_q = 15

a.u.),[62,64] and O ($\alpha_d = 5.41$ a.u., $\alpha_q = 16.90$ a.u.)[62,63] atoms (see Ref. 57 for further details).

C. Screening corrected additivity rule

In order to calculate the cross sections for electron and positron scattering from the C_4H_8O molecule, we then applied the additivity rule (AR) technique to our IAM results for each constituent atom. In this approach, the molecular scattering amplitude is derived from the sum of all the relevant atomic amplitudes, including the phase coefficients, thus leading to the molecular DCS for the molecule in question. ICS can then be determined by integrating those DCS, with the sum of the elastic ICS and absorption ICS (for all inelastic processes except rotations and vibrations) then giving the TCS. However, the AR does not take into account the molecular structure, so that it is really only applicable when the incident particles are so fast that they effectively "see" the target molecule as a sum of the individual atoms (typically above ~100 eV). In order to reduce this limitation, García and Blanco[51,65] introduced the SCAR method. This takes the geometry of the relevant molecule (atomic positions and bond lengths) into account by using some screening coefficients. With this correction the range of validity might be extended to impact energies of 30 eV or a little lower, at least as far as electron scattering is concerned. With respect to positron scattering, this lower energy limit still needs further study, particularly at the elastic DCS level.

D. Rotational excitations

From the above description of the IAM-SCAR procedure, it is clear that vibrational and rotational excitations are not considered in the present calculations. However, for polar molecules such as THF, additional dipole-induced excitation cross sections can be calculated following the procedure suggested by Jain.[66] Basically, in this approach, rotational excitation DCS and ICS for a free electric dipole are calculated in the framework of the first Born approximation (FBA), which can be incorporated into our IAM-SCAR calculation in an incoherent way, just by adding their results as an independent channel. Although rotational excitation energies are, in general, very small (typically a few meV) in comparison with the present incident energies, in order to validate the Born approximation the incident energies should be higher than about a few eV. Under these circumstances, rotational excitation cross sections $J \rightarrow J'$ were calculated by weighting the population for the Jth rotational quantum number at 300 K, and estimating the average excitation energy from the corresponding rotational constants.

In addition, when the permanent dipole moment of the molecule is significantly large, the FBA also fails for middle and large scattering angles. In order to partially overcome this limitation, we introduced a correction based on that suggested by Dickinson,[67] which brings a substantial improvement for electron and positron scattering cross sections with strongly polar molecules. This procedure introduces a first-order corrective term to the differential cross sections ($d\sigma^{Dck}/d\Omega$) for the middle and large angles, but maintains the FBA correction ($d\sigma^{B}/d\Omega$) for the forward scattering angles

$$\frac{d\sigma^{B}}{d\Omega} \approx \frac{\mu^2}{6E}\frac{1}{\sin^2(\theta/2)} \qquad \theta < \theta_c, \tag{5}$$

$$\frac{d\sigma^{Dck}}{d\Omega} \approx \frac{\pi\mu}{64E}\frac{1}{\sin^3(\theta/2)} \qquad \theta > \theta_c. \tag{6}$$

In Eqs. (5) and (6), μ is the permanent dipole moment of the molecule and E the incident energy. Provided that $\mu > 0.75$ D, both curves smoothly join together at $\theta = \theta_c$, i.e., the critical angle at which they cross each other.

IV. RESULTS AND DISCUSSION

A. Total cross sections

We show in Figure 2 the results of our TCS measurements for positron scattering from THF. We also list our numerical values in Table II, as a function of the positron energy, together with the overall error bars on the TCS. We clearly see in Figure 2 how dramatically the TCS increases in magnitude as the positron energy decreases. We have already observed in our earlier study on water and formic acid[12] this same kind of trend in the low-energy TCS for those polar species. Similar trends in TCS for polar polyatomic molecules have also been seen in the extensive studies from the University of Trento (see, for instance, Refs. 18, 22, and 68–70). We believe that this behaviour in the magnitude of the TCS at these lower energies is mostly due to the large permanent dipole moment and strong dipole polarizability of the target. In fact, both properties are expected to play an important role in the long-range dipole interaction, between the target molecule and the incident positrons, that dominates over the static interaction in the low-energy scattering process.

Also plotted in Figure 2 are the present measured TCS corrected for the forward angle scattering effect at a few selected energies, as well as the TCS computed with our IAM-SCAR approach, both with and without Born-dipole rotational excitations for positron collisions with THF. The results of our calculations are also reported in Table III. We note here that a physically consistent comparison can only be made between our measured data corrected for forward scattering and our TCS computed with the rotational excitations. This is because of the very forward peaked nature of the elastic DCS that also accounts for rotational excitations (see Sec. IV C): as the present experiment misses some of the forward angle scattering, our measurements are unlikely to account for this effect on the TCS. We see in Figure 2 that there is only a qualitative agreement between the present corrected experimental TCS and theoretical TCS that accounts for the rotational excitations. That calculation is much higher in magnitude than the corrected measured TCS, except above ~60 eV where it lies below the measured data. Note that we do not *a priori* expect our positron scattering model to be accurate at the lower energies, as it is at those energies where the SCAR method starts to fail (see Sec. III). Nonetheless, the disagreement we find between the theory and the experiment indicates that further improvement of the present theoretical approach is

TABLE III. The present TCS (σ_T), elastic (σ_E) and summed inelastic ICS (σ_I) (except rotations and vibrations) for positron scattering from THF calculated with our IAM-SCAR approach. Also given are the ICS for the Born dipole-induced rotational excitations (σ_{rot}) and the TCS that includes those cross sections (σ_{T+rot}).

Energy (eV)	σ_E (10^{-20} m^2)	σ_I (10^{-20} m^2)	σ_T (10^{-20} m^2)	σ_{rot} (10^{-20} m^2)	σ_{T+rot} (10^{-20} m^2)
1	67.49	0	67.49	121.81	189.30
1.5	52.65	0	52.65	85.41	138.06
2	46.76	0	46.76	66.09	112.85
3	41.16	0	41.16	46.20	87.36
4	36.68	0	36.68	35.84	72.52
5	33.32	0.11	33.43	29.29	62.72
7	27.58	1.24	28.82	21.61	50.43
10	14.51	20.36	34.87	15.77	50.64
15	11.26	25.09	36.35	10.75	47.10
20	10.50	25.59	36.09	8.29	44.38
30	9.74	24.53	34.27	5.71	39.98
40	9.10	23.16	32.26	4.45	36.71
50	8.48	21.90	30.38	3.61	33.99
70	7.36	19.77	27.13	2.66	29.79
100	6.08	17.39	23.47	1.90	25.37
150	4.68	14.56	19.24	1.32	20.56
200	3.81	12.60	16.41	1.01	17.42
300	2.78	9.97	12.75	0.70	13.45
400	2.20	8.29	10.49	0.53	11.02
500	1.83	7.11	8.94	0.42	9.36
700	1.38	5.57	6.95	0.31	7.26
1000	1.03	4.26	5.29	0.22	5.51
2000	0.57	2.41	2.98	0.11	3.09
3000	0.40	1.70	2.10	0.08	2.18
4000	0.31	1.32	1.63	0.06	1.69
5000	0.26	1.08	1.34	0.05	1.39

warranted. It might be argued that the discord between our most physical computation and our corrected TCS, could also suggest that our estimate of the correction for the forward angle scattering effect is actually too small at the lower energies. However, given that the angular discrimination of the present measurements is very well known, this would suggest that our theoretical DCS must be incorrect, which also hints at more development of our formalism being required. We also note a "dip" in our calculated TCS that seems to correspond with the opening of the first inelastic channel (Ps formation). As this "dip" is not observed in the Trento TCS data[22] (see below) nor in our measured TCS, we can only conclude that it is an artefact of the present computation. We finally see in Figure 2 that the behavior of our calculated TCS, without the rotational excitations, is similar to that of our uncorrected experimental results over most of the common energies. In fact, the overall level of accord between theory and experiment is quite good, often to within the total error bars on the present measured data. However, given the above discussion, this agreement is probably rather fortuitous.

The present experimental and theoretical TCS are also compared in Figure 2 to the only other TCS measurements due to the group at the University of Trento.[22] Our IAM-SCAR computations without Born-dipole rotational excitations are consistent with those previous results, to within the overall uncertainties on those measurements, up to ∼8 eV. Above that energy, however, the current calculated TCS tends to diverge from the results of Zecca *et al.*,[22] as it rises in magnitude owing to the increasing contribution of the inelastic channels. This may also partly be an effect of the angular discrimination affecting the Trento measurements. We also find a good level of accord between Zecca *et al.*[22] and our experimental TCS data from ∼1 eV to the Ps formation threshold energy, as the two data sets are consistent with each other to within their overall error bars. However, between E_{Ps} and about 20 eV our experimental TCS tends to diverge from the results of Zecca *et al.*[22] and is somewhat larger in magnitude. Indeed, the discrepancy is nearly 35% at about 20 eV. We were a little surprised by this result, as previous studies by the two groups on argon,[41,71] krypton,[42,72] and xenon[73,74] had shown a quite satisfactory level of accord between their "uncorrected" TCS. Indeed, Zecca *et al.*[69] noted that the angular discrimination of the Trento apparatus is comparable to that of the present spectrometer and since both independent measurements were conducted at the same temperature (∼24 ± 2 °C) it is reasonable to assume that the conformational distributions of the THF molecules in both measurements were also similar. While the purity of the present THF sample (>99.86%) is superior to that used in Trento (>99%), such a small difference is not expected to be able to explain the observed discrepancy above E_{Ps}. We therefore have no quantitative explanation for this observation at present, we simply note that the Trento TCS suggests a much smaller Ps formation cross section compared to that implied from the present TCS data and our direct measurement of the Ps formation cross section (see later in Sec. IV B).

TABLE IV. The present TCS for electron scattering from THF computed with our IAM-SCAR method, both without (σ_T) and with (σ_{T+rot}) the Born dipole-induced rotational excitation cross sections.

Energy (eV)	σ_T (10^{-20} m^2)	σ_{T+rot} (10^{-20} m^2)
1	79.53	201.34
1.5	74.21	159.62
2	68.61	134.70
3	58.53	104.73
4	54.61	90.45
5	51.81	81.10
7	47.32	68.93
10	43.20	58.97
15	40.21	50.96
20	38.87	47.16
30	36.80	42.51
40	34.67	39.12
50	32.68	36.29
70	29.40	32.06
100	25.76	27.66
150	21.62	22.94
200	18.79	19.80
300	15.09	15.79
400	12.69	13.22
500	10.98	11.40
700	8.71	9.02
1000	6.70	6.92
2000	3.84	3.95
3000	2.72	2.80
5000	1.74	1.79

In order to investigate any differences or similarities in the dynamics of positron and electron scattering from THF, we carried out additional calculations of the TCS for electron impact on THF with our IAM-SCAR approach, with and without Born-dipole rotational excitations. Those results are also plotted in Figure 2 and the numerical values are listed in Table IV. It is apparent from Figure 2 that the qualitative behaviour of our calculated positron and electron-impact TCS is very similar, with all TCS decreasing in magnitude with increasing incident energy. This suggests that the TCS are rather insensitive to the sign of the charge of the scattering probe and, hence, the low-energy scattering dynamics is mostly driven by the dipole interaction. However, we also note that the electron-impact TCS lie above the corresponding positron-impact results throughout the entire energy range covered by our computations. We had anticipated this outcome, as the main interactions that drive the low-energy electron-scattering process (the static and dipole interactions) are both attractive, whereas the static interaction becomes repulsive when positrons are the scattering probe. Additionally, at low energies, exchange scattering can be very important when electrons are the incident probe.

However, we had also expected our computations for positron and electron collisions with THF to converge around 100–200 eV, as the two main processes that differentiate positron and electron scattering, namely, Ps formation and the exchange interaction, become negligible at these higher energies. We see in Figure 2 that this is not the case here as the electron-impact TCS appear to be still slightly larger in magnitude than the corresponding positron-impact TCS, even above 200 eV. The reason for this unanticipated behaviour might lie in the fact that we employed different absorption potentials in our atomic optical models for positron and electron scattering. Note that the present measurements and the electron TCS from Możejko *et al.*[23] do merge at around 130 eV as expected. This suggests that further development of our IAM-SCAR approach is warranted, particularly, perhaps, in the positron case. It is also notable that the present measurements lie above our positron-impact calculated results including the rotational excitations above 120 eV, which also suggests more work on our positron scattering theory might be needed.

We finally compare, in Figure 2, the present measured and calculated positron and electron-impact TCS, with selected, earlier, electron-impact TCS. Specifically, we plot the electron *R*-matrix computations of Bouchiha *et al.*[32] together with the electron measurements of Możejko *et al.*,[23] as a comparison of those two data sets with the other existing experimental electron TCS results[22,24] has already been given in a recent paper.[24] In Figure 2, we see that the magnitude of all the various positron and electron-impact TCS can be quite different at the lower energies, although the TCS show very similar shapes, except for the results of Możejko *et al.*[23] below ~6 eV. Indeed, we note that the electron-impact TCS of Możejko *et al.*[23] lie below the present positron-impact TCS at energies below ~3 eV. This was somewhat unexpected, but can easily be explained in terms of the inferior angular discrimination of the electron experiment at Gdańsk with respect to that of the present measurements. Note that the importance of the angular discrimination effect on some of the TCS measurements of the Gdańsk group was observed earlier in the positron scattering studies at Trento on α-tetrahydrofurfuryl alcohol[68] and the cyclic ethers, ethylene oxide, and tetrahydropyran.[70]

B. Inelastic cross sections

The present experimental Ps formation cross sections are listed in Table II and plotted in Figure 3, together with their overall error bars. These are the first measurements of this cross section. We see in Figure 3 that the Ps formation cross section starts rising sharply at threshold and continues to increase markedly in magnitude with increasing positron energy until it reaches a maximum at around 15 eV. We note that, at this energy, the ratio of the Ps formation cross section to the TCS is also at its largest value. Above that energy the Ps formation cross section begins to decrease in magnitude, related to the direct ionization scattering channel becoming progressively dominant with increasing energy. The Ps formation cross section is observed to finally approach zero magnitude at about 160 eV, consistent with the merging of our measured positron TCS with the electron data at around that energy.

In Figure 3, we also plot our measurements of the summed ICS for electronic-state excitations and direct ionization of THF by positron impact. These numbers are also listed in Table II, and they also represent the first measurements of those cross sections. We note that the ground state ($^1A_1$) of the THF molecules is a singlet.[32] Therefore, the threshold

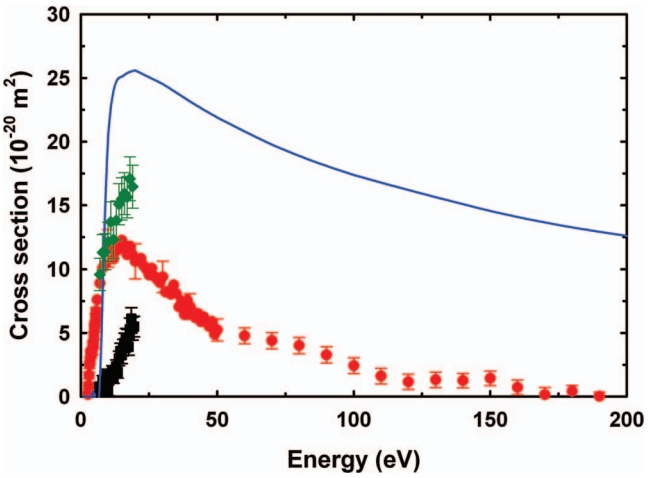

FIG. 3. The present measured Ps formation cross section (●) and summed inelastic ICS for electronic excitations and direct ionization (■). Also shown is the sum of the Ps formation cross section and the inelastic ICS (♦) at the common positron energies, in order to compare to the current IAM-SCAR computed sum over all inelastic ICS (———) except rotations and vibrations. Note that for clarity the overall error bars on the present experimental Ps formation cross sections between 6 and 50 eV are shown only at selected incident energies.

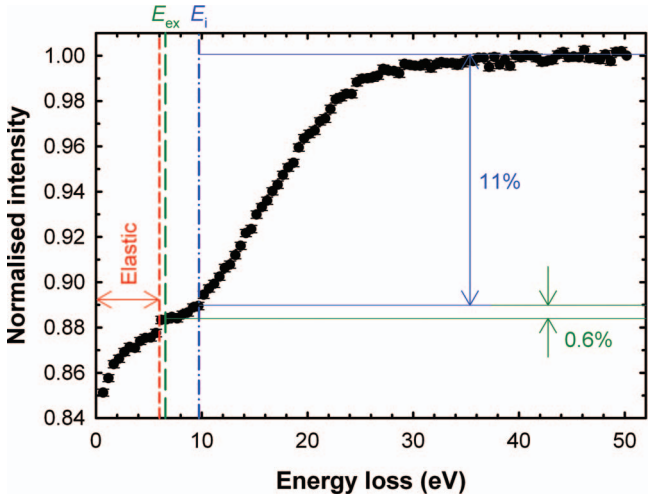

FIG. 4. Example of a RPA curve measured with THF vapour in the scattering cell at a scattering energy of 30 eV and with a ratio $B_{SC}/B_{RPA} = 5$. The red (– – –), green (— — —), and blue (– · – · – ·) vertical lines indicate the threshold energies for the end of the quasi-elastic scattering region, the first electronic singlet state and the first ionization potential in THF, respectively. Shown also are the estimates for the fraction of the inelastic to total scattering occurring between the opening of the first electronic excitation and the onset of direct ionization, as well as that taking place above the first ionization energy onwards.

energy for the first electronic singlet state in THF that can be excited by positrons, which is a part of a band of energetically low-lying Rydberg states, is $E_{ex} \approx 6.6$ eV.[30] In fact, we see in Figure 3 that the present inelastic ICS starts rising quite steeply at around that energy and continues to increase in magnitude with increasing incident energy until the limit of our measurements.

We now compare our experimental Ps formation cross section and sum over the inelastic ICS for electronic excitations and direct ionization, with the present theoretical results for the sum over the inelastic ICS for Ps formation, electronic excitations, and direct ionization. The theoretical results are also shown in Figure 3 and listed in Table III. We observe that the present summed inelastic ICS computed with our IAM-SCAR method starts rising dramatically at ∼7 eV, and peaks at 20 eV before decreasing in magnitude with increasing positron energy. The fact that the lowest inelastic process appears to open at ∼7 eV in our computation, is at odds with the current experimental Ps formation cross section results which are consistent with the known threshold energy for that scattering channel. Therefore, this observation probably reflects a limitation in our IAM-SCAR approach. In addition, we also see in Figure 3 that between ∼8 and 20 eV our calculation somewhat overestimates the magnitude of the sum over the measured inelastic ICS.

In our experimental configuration, information about inelastic scattering occurring at a given incident energy can also be obtained by carrying out a retarding potential analysis of the positron beam with the THF vapour present in the scattering cell and by employing a suitable magnetic field ratio B_{SC}/B_{RPA} (see Sec. II). In particular, this analysis allows us to estimate the fraction of the elastic or inelastic to total scattering that takes place at a given incident energy and also to localize the threshold energies for the first electronic state and the first ionization potential of the target molecule. An example of such a RPA curve measured at a scattering energy of 30 eV and with a ratio $B_{SC}/B_{RPA} = 5$ is given in Figure 4. We can clearly see a small step in the RPA curve at the energy loss of ∼6 eV which indicates the end of the energy range where only elastic scattering occurs (if we neglect vibrations and rotations). Nearly 88.4% of the total scattering that occurs at the scattering energy of 30 eV is thus due to the elastic channel. All of the scattering that occurs above the energy loss of ∼6 eV is entirely due to the various inelastic scattering processes that become open with increasing positron energy. In Figure 4, we indicate with a green and a blue vertical bar, the threshold energies for the first electronic singlet state ($^1B_1$) and the first ionization potential of THF, respectively. The effect of the opening of the scattering channels corresponding to each of these two inelastic processes is clearly visible in Figure 4 as a change in the slope of the RPA curve in the proximity of the process thresholds. Any scattering events that occur in the energy loss region between these two thresholds are exclusively due to the excitation of the low-lying electronic singlet states of THF, whereas those occurring above the first IP are due to direct ionization and the excitation of the higher-lying electronic states of THF. In Figure 4, the majority of the rise in the RPA curve appears to happen after the first IP, which suggests that most of the TCS at 30 eV might be due to direct ionization.

C. Elastic differential cross sections

The present, measured quasi-elastic DCS for positron impact with THF, at incident energies between 1 and 25 eV, are reported in Table V. Those DCS are also shown in Figure 5 at selected energies only. It is worth noting here that in our experimental technique positrons scattered in the backward

TABLE V. The present measured elastic DCS for positron collisions with THF, as a function of the scattering angle at the incident positron energies investigated. Also shown are the overall error bars.

	DCS (10^{-20} m^2 sr^{-1})					
	1 eV		2 eV		5 eV	
Angle (deg)	Average	Error	Average	Error	Average	Error
7.9						
12.7						
17.7			50.78	4.78	27.81	2.32
22.6	62.78	6.28	31.73	3.18	18.77	1.84
27.6	44.71	4.50	28.98	2.83	10.84	1.54
32.6	35.15	3.55	17.23	1.92	4.94	1.31
37.5	27.30	2.78	11.74	1.49	4.14	1.19
42.5	22.06	2.26	10.48	1.33	3.59	1.07
47.5	17.48	1.82	7.68	1.14	2.30	0.97
52.5	13.26	1.41	5.12	0.96	2.86	0.90
57.4	9.39	1.05	4.95	0.92	3.85	0.85
62.4	6.82	0.83	2.95	0.83	2.02	0.80
67.4	5.24	0.70	1.01	0.75	1.97	0.76
72.3	2.29	0.51	1.82	0.75	1.51	0.75
77.3	2.08	0.49	2.28	0.75	1.67	0.73
82.1	1.53	0.48	0.58	0.74	2.05	0.77
86.5	0.84	0.61	0.54	0.97	−0.67	1.01
	DCS (10^{-20} m^2 sr^{-1})					
	6 eV		8 eV		10 eV	
Angle (deg)	Average	Error	Average	Error	Average	Error
7.9						
12.7	46.83	2.20	159.61	3.54	46.85	0.94
17.7	24.96	1.50	27.26	2.10	17.15	0.65
22.6	14.74	1.16	9.46	1.63	8.24	0.52
27.6	8.09	0.95	6.39	1.34	4.12	0.43
32.6	4.37	0.80	3.21	1.16	2.31	0.37
37.5	1.91	0.72	2.20	1.04	2.25	0.33
42.5	3.33	0.65	3.39	0.94	1.96	0.30
47.5	2.58	0.59	4.07	0.86	2.08	0.27
52.5	1.95	0.54	1.36	0.81	1.57	0.25
57.4	3.12	0.52	2.16	0.74	1.51	0.24
62.4	2.67	0.50	1.43	0.72	0.96	0.23
67.4	1.17	0.46	3.03	0.69	0.95	0.22
72.3	2.07	0.46	1.40	0.70	0.50	0.21
77.3	1.46	0.46	−0.29	0.66	0.21	0.21
82.1	0.38	0.46	1.85	0.67	0.35	0.22
86.5	0.59	0.62	−1.45	0.89	0.13	0.28
	DCS (10^{-20} m^2 sr^{-1})					
	15 eV		20 eV		25 eV	
Angle (deg)	Average	Error	Average	Error	Average	Error
7.9					128.40	1.82
12.7	48.53	2.86	24.48	0.65	20.91	0.62
17.7	11.73	1.39	9.42	0.40	7.09	0.42
22.6	5.39	1.05	3.31	0.29	3.33	0.32
27.6	3.19	0.87	2.24	0.24	1.33	0.26
32.6	2.21	0.74	1.60	0.21	1.89	0.23
37.5	1.92	0.65	1.74	0.19	0.79	0.20
42.5	2.23	0.59	1.06	0.17	1.03	0.18
47.5	1.59	0.54	0.83	0.15	0.28	0.17
52.5	1.14	0.49	0.58	0.14	0.49	0.15
57.4	1.46	0.48	0.51	0.13	0.45	0.14
62.4	1.08	0.45	0.55	0.13	0.27	0.14
67.4	0.42	0.43	0.34	0.12	0.30	0.13
72.3	0.61	0.42	0.19	0.12	0.32	0.13
77.3	0.39	0.41	0.40	0.12	0.35	0.12
82.1	−0.62	0.43	0.33	0.12	0.04	0.13
86.5	1.79	0.57	−0.08	0.16	0.30	0.17

direction (i.e., through angles greater than 90°) are reflected from the potential barriers associated with the trap and other elements, and can travel back through the gas cell.[42,43] As a result, the measured cross section at any angle θ is actually folded about 90°, with the angles θ and $180^\circ - \theta$ summed. Therefore, any electron experimental DCS and all the theoretical DCS plotted in Figure 5 are also folded in order to enable a genuine comparison with the current experimental data. In addition, as anticipated in Sec. II, we cannot make measurements of the cross sections in the angular range $0^\circ \pm \theta_{\min}$, where $\theta_{\min}$ is the missing angle (see Table I). This is reflected in the DCS we report here. At a few of the scattering angles in Table V, a negative DCS is reported, which is of course unphysical. In those cases, we are simply dealing with small cross sections and in all but two the error bars allow for a physically sensible positive value. Note that all the statistical errors are at a one standard deviation level.

A common feature that emerges from Figure 5 is that the elastic DCS, at all investigated energies, dramatically rise in magnitude from 90° towards the more forward scattering angles. However, the most interesting aspect is how those DCS become progressively more forward peaked as the incident positron energy decreases from 25 to 1 eV. We had anticipated this result owing to the strongly polar nature of THF, as the relatively large dipole polarizability and permanent dipole moment of THF are expected to play an important role in the low-energy positron scattering dynamics.

We list in Table VI our elastic DCS for positron scattering from THF, as computed with our IAM-SCAR approach with Born dipole-induced rotational excitations, and we also plot those results in Figure 5 at the same energies as our measured DCS. We see in Figure 5 that there is, in general, reasonable qualitative agreement between our calculated DCS and the present experimental data at all investigated energies. This level of accord is also quantitatively fairly good at energies above ∼6 eV, where the level of agreement is particularly good at the larger angles although it becomes worse as one goes towards the more forward angles. The reason for these latter observations is that we do not expect our IAM-SCAR computations to be quantitatively valid at low energies.

As, to the best of our knowledge, the present experimental and theoretical positron elastic DCS results are unique, we also compare them to the corresponding electron-impact DCS available in the literature.[24–29,33–35] Given that the level of accord between the various electron DCS is, in general, very good at each energy, for the sake of clarity we only show in

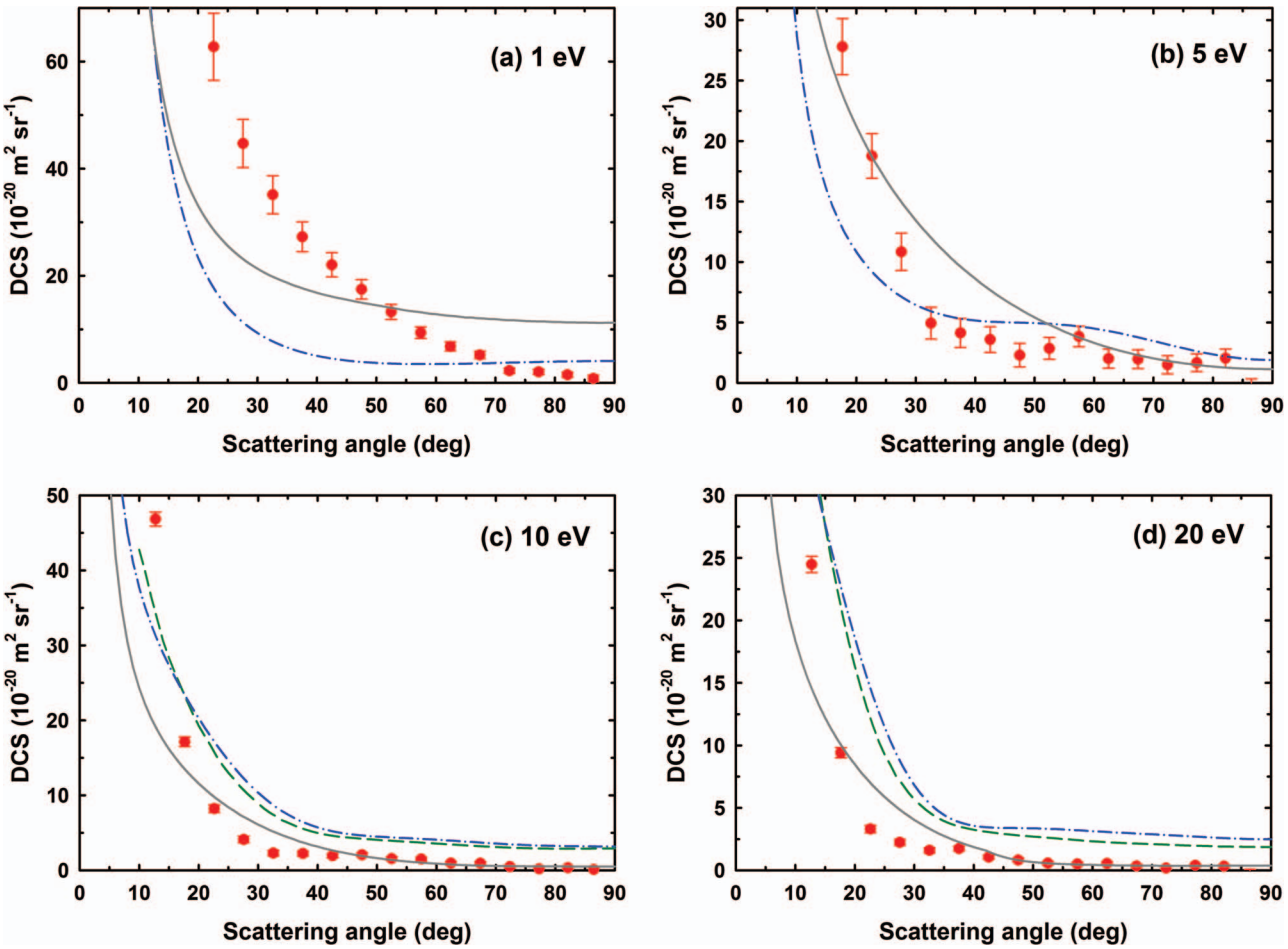

FIG. 5. The present measured (●) and calculated (———) quasi-elastic DCS for positron collisions with THF at selected incident energies: (a) 1 eV, (b) 5 eV, (c) 10 eV and (d) 20 eV. We show the present IAM-SCAR results that include the contribution of rotational excitations in order to consistently compare to our measured quasi-elastic DCS (see text). Plotted also are the electron-impact DCS results from the measurements of Allan[26] (— — —) and the SMC computations with Born-dipole correction of Gauf *et al.*[29] (– · – · – ·).

TABLE VI. The present elastic DCS for positron scattering from THF calculated with our IAM-SCAR approach, with Born dipole-induced rotational excitations, at selected scattering energies.

	DCS (10^{-20} m^2 sr^{-1})							
Angle (deg)	1 eV	2 eV	5 eV	7 eV	10 eV	15 eV	20 eV	30 eV
0	2.80×10^9	2.67×10^9	6.69×10^9	9.35×10^9	1.34×10^{10}	2.01×10^{10}	2.67×10^{10}	4.00×10^{10}
10	88.77	53.77	39.48	36.96	24.05	19.24	18.29	18.17
20	28.56	21.67	20.53	19.15	11.31	8.90	8.40	7.95
30	16.80	13.95	12.80	10.95	5.82	4.34	3.95	3.50
40	12.24	10.08	8.04	6.05	2.88	2.02	1.78	1.00
50	9.83	7.62	4.90	3.19	1.33	0.88	0.57	0.50
60	8.04	5.71	2.86	1.55	0.60	0.34	0.33	0.29
70	6.89	4.37	1.61	0.75	0.29	0.26	0.24	0.20
80	6.13	3.42	0.92	0.38	0.24	0.24	0.21	0.15
90	5.63	2.78	0.57	0.30	0.26	0.23	0.19	0.11
100	5.24	2.33	0.43	0.32	0.29	0.23	0.16	0.09
110	5.01	2.04	0.42	0.38	0.30	0.21	0.13	0.07
120	4.82	1.86	0.46	0.45	0.31	0.18	0.11	0.06
130	4.68	1.76	0.52	0.52	0.30	0.16	0.10	0.06
140	4.59	1.71	0.59	0.58	0.29	0.14	0.09	0.06
150	4.54	1.69	0.64	0.64	0.28	0.13	0.08	0.06
160	4.54	1.69	0.69	0.68	0.27	0.13	0.08	0.06
170	4.48	1.70	0.72	0.71	0.26	0.12	0.08	0.06
180	4.48	1.70	0.73	0.72	0.26	0.12	0.08	0.06

Figure 5 the experimental results from Allan[26] and the theoretical results of Gauf *et al*.[29] First, we observe in Figure 5 that the existing electron-impact elastic DCS are strongly forward peaked, similar to the present measured and computed positron-impact DCS. This suggests that the dipole interaction dominates over the static interaction in the scattering process at the lower energies. Second, we also note that while there is generally good qualitative agreement between the positron and electron-impact DCS, they usually differ in terms of their magnitude. Whereas the positron DCS seems to be larger in magnitude, than the corresponding electron DCS, at the forward angles below ~6 eV (see Figures 5(a) and 5(b)), they tend to become lower in magnitude above that energy (see Figures 5(c) and 5(d)). The results below 6 eV are also surprising to us, but as we have discussed possible causes for this effect in Sec. IV A we do not revisit the issue again here.

V. CONCLUSIONS

In this paper, we have presented absolute experimental measurements of the TCS, Ps formation cross section, summed inelastic ICS for electronic-state excitations and direct ionization, and quasi-elastic DCS for positron scattering from THF at impact energies from 1 to 190 eV. In addition, we have also presented positron and electron-impact TCS and ICS results from our IAM-SCAR computations between 1 and 5000 eV, as well as some positron quasi-elastic DCS for energies below 30 eV. A reasonable level of accord was found between the present measured and calculated positron-impact TCS over most of the common energy range. A quantitative level of agreement was also found between our results and the earlier positron TCS measurements by Zecca *et al*.[22] below E_{Ps}. The present inelastic ICS are the first experimental and theoretical results for this target. In an attempt to gain some insight into the fundamental interactions driving the low-energy scattering of positrons and electrons from THF, we also compared our positron-impact cross sections to the existing electron-impact results from the literature. We typically found a good qualitative level of accord between the positron and electron-impact cross sections, which suggests that the dipole interaction plays a dominant role in the scattering dynamics at low energy.

ACKNOWLEDGMENTS

The authors gratefully acknowledge the Australian Research Council (ARC) Centres of Excellence Program for funding. C.M. is also grateful to the ARC for financial support under the Australian Postdoctoral Fellowship program. G.G. and F.B. would like to acknowledge the Spanish Ministerio de Economía y Productividad (Project No. FIS2009-10245) and the European Science Foundation (COST Action MP1002 – Nano-IBCT) for financial support. L.C. would like to thank Antonio Zecca for his useful comments. The authors also thank Leigh Hargreaves for providing data in numerical form. Finally, we all thank the technical staff at the ANU, Stephen Battiston and Ross Tranter, for their invaluable input.

[1] L. Chiari, M. J. Brunger, and A. Zecca, *Radiation Damage in Biomolecular Systems*, edited by G. García Gómez-Tejedor and M. C. Fuss (Springer, Berlin, 2012), p. 155.
[2] B. Boudaiffa, P. Cloutier, D. Hunting, M. A. Huels, and L. Sanche, Science **287**, 1658 (2000).
[3] F. Martin, P. D. Burrow, Z. Cai, P. Cloutier, D. Hunting, and L. Sanche, Phys. Rev. Lett. **93**, 068101 (2004).
[4] A.-C. Hassan, P.-C. Dugal, and L. Sanche, Radiat. Res. **153**, 23 (2000).
[5] H. Abdoul-Carime, S. Gohlke, and E. Illenberger, Phys. Rev. Lett. **92**, 168103 (2004).
[6] P. L. Levesque, M. Michaud, and L. Sanche, J. Chem. Phys. **122**, 094701 (2005).
[7] M. J. Brunger, S. J. Buckman, and A. Zecca, J. Phys.: Conf. Ser. **194**, 012034 (2009).
[8] T. Van Vliet, H. J. M. van Dijk, P. Zoon, and P. Walstra, Colloid Polym. Sci. **269**, 620 (1991).
[9] A. Bögershausen, S. J. Pas, A. J. Hill, and H. Koller, Chem. Mater. **18**, 664 (2006).
[10] L. Menichetti, L. Cionini, W. A. Sauerwein, S. Altieri, O. Solin, H. Minn, and P. A. Salvadori, Appl. Radiat. Isot. **67**, S351 (2009).
[11] E. Surdutovich, G. Setzler, W. E. Kauppila, S. J. Rehse, and T. S. Stein, Phys. Rev. A **77**, 054701 (2008).
[12] C. Makochekanwa, A. Banković, W. Tattersall, A. Jones, P. Caradonna, D. S. Slaughter, K. Nixon, M. J. Brunger, Z. Petrović, J. P. Sullivan, and S. J. Buckman, New J. Phys. **11**, 103036 (2009).
[13] M. Lepage, S. Letarte, M. Michand, F. Motte-Tollet, M.-J. Hubin-Franskin, D. Roy, and L. Sanche, J. Chem. Phys. **109**, 5980 (1998).
[14] D. Antic, L. Parenteau, and L. Sanche, J. Chem. Phys. B **104**, 4711 (2000).
[15] A. R. Milosavljević, A. Giuliani, M.-J. Hubin-Franskin, and B. P. Marinković, *Book of Abstracts of the 22nd Summer School and International Symposium of Ionised Gases*, edited by T. Grozdanov, Lj. Hadzievski, and N. Bibic (Vinca Institute of Nuclear Sciences Press, Belgrade, 2004), p. 69.
[16] B. Thiemer, J. R. Andreesen, and T. Schräder, Arch. Microbiol. **179**, 266 (2003).
[17] D. Antic, L. Parenteau, M. Lepage, and L. Sanche, J. Phys. Chem. B **103**, 6611 (1999).
[18] A. Zecca, L. Chiari, A. Sarkar, and M. J. Brunger, J. Phys. B **41**, 085201 (2008).
[19] D. Bouchiha, J. D. Gorfinkiel, L. G. Caron, and L. Sanche, J. Phys. B **40**, 1259 (2007).
[20] B. Cadioli, E. Gallinella, C. Coulombeau, H. Jobic, and G. Berthier, J. Phys. Chem. **97**, 7844 (1993).
[21] A. Giuliani, P. Limão-Vieira, D. Duflot, A. R. Milosavljević, B. P. Marinković, S. V. Hoffmann, N. Mason, J. Delwiche, and M.-J. Hubin-Franskin, Eur. Phys. J. D **51**, 97 (2009).
[22] A. Zecca, C. Perazzolli, and M. J. Brunger, J. Phys. B **38**, 2079 (2005).
[23] P. Możejko, E. Ptasińska-Denga, A. Domaracka, and C. Szmytkowski, Phys. Rev. A **74**, 012708 (2006).
[24] W. Y. Baek, M. Bug, H. Rabus, E. Gargioni, and B. Grosswendt, Phys. Rev. A **86**, 032702 (2012).
[25] A. R. Milosavljević, A. Giuliani, D. Šević, M.-J. Hubin-Franskin, and B. P. Marinković, Eur. Phys. J. D **35**, 411 (2005).
[26] M. Allan, J. Phys. B **40**, 3531 (2007).
[27] C. J. Colyer, V. Vizcaino, J. P. Sullivan, M. J. Brunger, and S. J. Buckman, New J. Phys. **9**, 41 (2007).
[28] M. Dampc, A. R. Milosavljevic, I. Linert, B. P. Marinković, and M. Zubek, Phys. Rev. A **75**, 042710 (2007).
[29] A. Gauf, L. R. Hargreaves, A. Jo, J. Tanner, M. A. Khakoo, T. Walls, C. Winstead, and V. McKoy, Phys. Rev. A **85**, 052717 (2012).
[30] T. P. T. Do, M. Leung, M. Fuss, G. Garcia, F. Blanco, K. Ratnavelu, and M. J. Brunger, J. Chem. Phys. **134**, 144302 (2011).
[31] M. Fuss, A. Muñoz, J. C. Oller, F. Blanco, D. Almeida, P. Limão-Vieira, T. P. D. Do, M. J. Brunger, and G. García, Phys. Rev. A **80**, 052709 (2009).
[32] D. Bouchiha, J. D. Gorfinkiel, L. G. Caron, and L. Sanche, J. Phys. B **39**, 975 (2006).
[33] P. Możejko and L. Sanche, Radiat. Phys. Chem. **73**, 77 (2005).
[34] C. S. Trevisan, A. E. Orel, and T. N. Rescigno, J. Phys. B **39**, L255 (2006).
[35] C. Winstead and V. McKoy, J. Chem. Phys. **125**, 074302 (2006).
[36] S. Tonzani and C. H. Greene, J. Chem. Phys. **125**, 094504 (2006).
[37] J. P. Sullivan, A. Jones, P. Caradonna, C. Makochekanwa, and S. J. Buckman, Rev. Sci. Instrum. **79**, 113105 (2008).
[38] S. J. Gilbert, C. Kurz, R. G. Greaves, and C. M. Surko, Appl. Phys. Lett. **70**, 1944 (1997).

[39]T. Takaishi and Y. Sensui, Trans. Faraday Soc. **59**, 2503 (1963).
[40]Centers for Disease Control and Prevention, National Institute for Occupational Safety and Health Publication No. 2005-149 (U.S. Department of Health and Human Services, Atlanta, 2007), see http://www.cdc.gov/niosh/docs/2005-149/pdfs/2005-149.pdf.
[41]A. C. L. Jones, C. Makochekanwa, P. Caradonna, D. S. Slaughter, J. R. Machachek, R. P. McEachran, J. P. Sullivan, S. J. Buckman, A. D. Stauffer, I. Bray, and D. V. Fursa, Phys. Rev. A **83**, 032701 (2011).
[42]C. Makochekanwa, J. R. Machacek, A. C. L. Jones, P. Caradonna, D. S. Slaughter, R. P. McEachran, J. P. Sullivan, S. J. Buckman, S. Bellm, B. Lohmann, D. V. Fursa, I. Bray, D. W. Mueller, A. D. Stauffer, and M. Hoshino, Phys. Rev. A **83**, 032721 (2011).
[43]J. P. Sullivan, S. J. Gilbert, J. P. Marler, R. G. Greaves, S. J. Buckman, and C. M. Surko, Phys. Rev. A **66**, 042708 (2002).
[44]K. Kimura, S. Katsumata, Y. Achiba, T. Yamazaki, and S. Iwata, *Handbook of He I Photoelectron Spectra of Fundamental Organic Molecules* (Japan Scientific Societies Press, Tokyo, 1981).
[45]J. P. Sullivan, C. Makochekanwa, A. Jones, P. Caradonna, D. S. Slaughter, J. Machacek, R. P. McEachran, D. W. Mueller, and S. J. Buckman, J. Phys. B **44**, 035201 (2011).
[46]A. Hamada and O. Sueoka, J. Phys. B **27**, 5055 (1994).
[47]P. Caradonna, J. P. Sullivan, A. Jones, C. Makochekanwa, D. S. Slaughter, D. W. Mueller, and S. J. Buckman, Phys. Rev. A **80**, 060701 (2009).
[48]F. Blanco and G. García, Phys. Lett. A **295**, 178 (2002).
[49]F. Blanco and G. García, Phys. Rev. A **67**, 022701 (2003).
[50]F. Blanco and G. García, Phys. Lett. A **317**, 458 (2003).
[51]F. Blanco and G. García, Phys. Lett. A **330**, 230 (2004).
[52]M. E. Riley and D. G. Truhlar, J. Chem. Phys. **63**, 2182 (1975).
[53]X. Z. Zhang, J. F. Sun, and Y. F. Liu, J. Phys. B **25**, 1893 (1992).
[54]G. Staszewska, D. W. Schwenke, D. Thirumalai, and D. G. Truhlar, Phys. Rev. A **28**, 2740 (1983).
[55]O. Zatsarinny, K. Bartschat, G. Garcia, F. Blanco, L. R. Hargreaves, D. B. Jones, R. Murrie, J. R. Brunton, M. J. Brunger, M. Hoshino, and S. J. Buckman, Phys. Rev. A **83**, 042702 (2011).
[56]R. P. McEachran, J. P. Sullivan, S. J. Buckman, M. J. Brunger, M. C. Fuss, A. Muñoz, F. Blanco, R. D. White, Z. Lj. Petrović, P Limão-Vieira, and G. García, J. Phys. B **45**, 045207 (2012).
[57]L. Chiari, A. Zecca, S. Girardi, E. Trainotti, G. García, F. Blanco, R. P. McEachran, and M. J. Brunger, J. Phys. B **45**, 215206 (2012).
[58]L. Chiari, P. Palihawadana, J. R. Machacek, C. Makochekanwa, G. García, F. Blanco, R. P. McEachran, M. J. Brunger, S. J. Buckman, and J. P. Sullivan, J. Chem. Phys. **138**, 074302 (2013).
[59]M. Charlton and J. W. Humberston, *Positron Physics* (Cambridge University Press, Cambridge, 2001).
[60]D. D. Reid and J. M. Wadehra, J. Phys. B **29**, L127 (1996).
[61]R. P. McEachran, D. L. Morgan, A. G. Ryman, and A. D. Stauffer, J. Phys. B **10**, 663 (1977).
[62]T. M. Miller and B. Bederson, Adv. At. Mol. Phys. **13**, 1 (1977).
[63]E.-A. Reinsch and W. Meyer, Phys. Rev. A **18**, 1793 (1978).
[64]A. K. Bhatia, *Positron Interactions with Atoms and Ions* (NASA's Goddard Space Flight Center, Maryland, 2012), see http://ntrs.nasa.gov/archive/nasa/casi.ntrs.nasa.gov/20120011692_2012010939.pdf.
[65]F. Blanco and G. García, J. Phys. B **42**, 145203 (2009).
[66]A. Jain, J. Phys. B **21**, 905 (1988).
[67]A. S. Dickinson, J. Phys. B **10**, 967 (1977).
[68]A. Zecca, L. Chiari, G. García, F. Blanco, E. Trainotti, and M. J. Brunger, New J. Phys. **13**, 063019 (2011).
[69]A. Zecca, L. Chiari, A. Sarkar, and M. J. Brunger, New J. Phys. **13**, 115001 (2011).
[70]A. Zecca, E. Trainotti, L. Chiari, M. H. F. Bettega, S. d'A. Sanchez, M. T. do N. Varella, M. A. P. Lima, and M. J. Brunger, J. Chem. Phys. **136**, 124305 (2012).
[71]A. Zecca, L. Chiari, E. Trainotti, D. V. Fursa, I. Bray, A. Sarkar, S. Chattopadhyay, K. Ratnavelu, and M. J. Brunger, J. Phys. B **45**, 015203 (2012).
[72]A. Zecca, L. Chiari, E. Trainotti, D. V. Fursa, I. Bray, and M. J. Brunger, Eur. Phys. J. D **64**, 317 (2011).
[73]J. R. Machacek, C. Makochekanwa, A. C. L. Jones, P. Caradonna, D. S. Slaughter, R. P. McEachran, J. P. Sullivan, S. J. Buckman, S. Bellm, B. Lohmann, D. V. Fursa, I. Bray, D. W. Mueller, and A. D. Stauffer, New J. Phys. **13**, 125004 (2011).
[74]A. Zecca, L. Chiari, E. Trainotti, and M. J. Brunger, J. Phys. B **45**, 085203 (2012).